Aquat Geochem
DOI 10.1007/s10498-011-9127-2

ORIGINAL PAPER

Aragonite Kinetics in Dilute Solutions

Christopher S. Romanek · John W. Morse · Ethan L. Grossman

Received: 13 July 2010 / Accepted: 25 March 2011

Abstract Aragonite was synthesized inorganically using a seeded-growth technique to characterize precipitation kinetics for the heterogeneous growth of solid from dilute solutions (ionic strength: 0.05–0.07 mol l^{-1}). The concentration of all aqueous constituents, including Ca ($\sim$5–15 mmol l^{-1}), Na ($\sim$10–35 mmol l^{-1}), Cl ($\sim$30–35 mmol l^{-1}), and carbon (as total alkalinity: $\sim$10 to 17 meq l^{-1}), was held constant by the addition of titrants that contained excess solute concentrations to balance the growth of solid phase during the precipitation reaction, and a CO_2/N_2 gas mixture (0.009–0.178) was bubbled through each solution to facilitate mass exchange between gaseous and aqueous carbon species. Forty-three experiments were conducted at 10° ($n = 13$), 25° ($n = 21$), and 40°C ($n = 9$), over a range of average saturation states with respect to aragonite from 8.3 to 28.5, 2.9 to 19.6 and 2.0 to 12.2, and average precipitation rates from $10^{2.8}$ to $10^{3.8}$, $10^{2.3}$ to $10^{4.0}$, and $10^{2.5}$ to $10^{4.1}$ micromol m^{-2} h^{-1}, respectively. Reaction orders averaged 1.7 $\pm$ 0.10 at 10°, 1.7 $\pm$ 0.07 at 25° and 1.5 $\pm$ 0.06 at 40°, and they were independent of temperature while rate constants averaged $10^{1.3}$ $\pm$ 0.12, $10^{1.9}$ $\pm$ 0.06, and $10^{2.6}$ $\pm$ 0.04 micromol m^{-2} h^{-1}, respectively, increasing one-half order of magnitude for each 15°C rise in temperature. From these data, an Arrhenius activation energy of 71.2 kJ mol^{-1} is calculated for the heterogeneous precipitation of aragonite. This value is comparable to a sole independent measurement of 80.7 kJ mol^{-1} reported for the solid-solution recrystallization of monohydrocalcite to aragonite (Munemoto and Fukushi in J Mineral Petrol Sci 103: 345–349, 2008).

This paper is dedicated to John W. Morse, who thoughtfully guided this research prior to his passing.

C. S. Romanek (✉)
NASA Astrobiology Institute and Department of Earth and Environmental Sciences, University of Kentucky, Lexington, KY 40506, USA
e-mail: c.romanek@uky.edu

J. W. Morse
Department of Oceanography, Texas A&M University, College Station, TX 77843, USA

E. L. Grossman
Department of Geology and Geophysics, Texas A&M University, College Station, TX 77843, USA

Published online: 03 May 2011

Keywords Aragonite · Precipitation rate · Activation energy · Kinetics

1 Introduction

Calcium carbonate precipitation kinetics are important to a diverse group of scientific interests including the following: the chemical state of the world's oceans (Morse and Berner 1972; Berner et al. 1978; Morse et al. 2006), the mass transport of dissolved carbonate during chemical diagenesis (Morse and Mackenzie 1993; Lee and Morse 1999; Wiltschko and Morse 2001), the evolution of secondary porosity in carbonate rocks (Scholle and Halley 1985; Morse et al. 1997), and the implications of trace element partitioning in carbonate phases (Mucci and Morse 1990). More pragmatic concerns include controlling carbonate precipitation during desalinization (Elliot 1969; Morse et al. 1979; Omar et al. 2009), geothermal energy production (Arnorsson 1979; Amjad 1987), and waste treatment (Reddy 1978). More recently, aragonite precipitation kinetics have been studied to estimate and manipulate the growth rate of biogenic skeletal tissues (e.g., otoliths: Romanek and Gauldie 1996; restorative and osseous surgeries: Oudadesse et al. 2004) and to effectively control the growth forms of aragonite for coatings and fillers in various industrial applications (Hu and Deng 2003, 2004).

Early precipitation kinetic studies utilized the free-drift technique where solution chemistry drifts toward equilibrium from an initial state of supersaturation after the spontaneous nucleation of a solid phase (homogeneous nucleation; e.g., Packter 1968) or nucleation on seed material (heterogeneous nucleation; e.g., Nancollas and Reddy 1971). Both homogeneous and heterogeneous nucleation can influence the early stages of crystal growth and give rise to variable reaction kinetics, depending on the initial conditions of precipitation. Free-drift seeded-growth experiments were developed to circumvent this problem by precipitating solid carbonate heterogeneously as an overgrowth on seed material. With this method, $CaCO_3$ is precipitated over a continuum of precipitation rates. The rate constant determined from such experiments is calculated from the rate of change of solution chemistry with respect to time. As with spontaneous-nucleation experiments, free-drift seeded-growth experiments have a constantly changing solution chemistry in which a solid phase of (potentially) changing stoichiometry may be produced. In extreme cases, differing solid phases may be thermodynamically stable over the course of an experimental run (Tai and Chen 1998; Elfil and Roques 2004; Kawano et al. 2009).

To maintain constant solution chemistry, the chemo-stat technique was developed by Kazmierczak et al. (1982). Carbonate precipitation is monitored in a solution at a steady state of chemical disequilibrium, allowing for the independent control of physical and chemical variables that potentially alter precipitation rate over a wide range of saturation states. This method can be employed to monitor solution conditions for an extended period of time as opposed to free-drift and spontaneous-nucleation experiments. Since the chemistry remains constant throughout a run, a solid of constant stoichiometry is formed that experiences only a single set of physical and chemical conditions. Mineralogically pure seed material used as a substrate for heterogeneous crystal growth, minimizes the possibility of multiple growth mechanisms. Finally, bubbling a CO_2/N_2 gas mixture through a solution facilitates the mass exchange of gaseous and aqueous carbon species and promotes thermodynamic equilibrium between phases.

Only a handful of studies have used the chemo-stat technique to characterize carbonate crystallization kinetics (e.g., Busenberg and Plummer 1986; Walter 1986; Burton 1988),

and of those, none have determined the effect of temperature on the precipitation kinetics of aragonite. Since aragonite forms under a wide range of conditions, the characterization of aragonite precipitation kinetics in dilute solutions may provide valuable insights into reaction mechanisms that occur within many environments.

A series of laboratory experiments was undertaken to better understand the factors that influence the heterogeneous growth of aragonite from dilute solutions using the chemo-stat technique. Forty-three experiments were conducted, in which the effects of temperature, saturation state, and solution PCO_2 are documented on precipitation rate.

2 Materials

2.1 Solutions

Fisher Certified chemicals were used to make stock solutions containing $NaHCO_3$, $CaCl_2{\cdot}2H_2O$, and distilled deionized water (DDW) in concentrations that ranged from 10 to 15 meq l^{-1} and 5 to 15 mmol l^{-1}, respectively. In a few instances, NaCl was added to raise the ionic strength of the stock solution $\sim$0.05 mol l^{-1}. Water-saturated pure CO_2 was bubbled through DDW prior to the dissolution of the reagents to ensure that all salts solutions remained in the aqueous phase and that the solution remained undersaturated with respect to $CaCO_3$ prior to an experimental run. After bubbling with CO_2 for at least 24 h, one-half liter aliquots of stock solution were placed in 500-ml bottles and sealed with gas tight (poly-seal cap) lids for later use.

2.2 Gases

Specified CO_2/N_2 gas mixtures were bubbled through aliquots of stock solution during the experimental runs. Gas mixtures were made by mixing known molar quantities of pure CO_2 and N_2 in an evacuated gas tank. Calculated CO_2/N_2 ratios were identical to the analysis of gas mixtures made using standard gas chromatography techniques.

2.3 Solids

Aragonite seed material was used in each experiment. The seed was precipitated by slowly adding 200 ml of a 1.0 mol l^{-1} $CaCl_2{\cdot}2H_2O$ solution to 2.0 l of a 0.1 mol l^{-1} Na_2CO_3 solution at 85°C (Wray and Daniels 1957). The solid was filtered, washed with DDW, and freeze-dried. Scanning electron photomicrographs (Fig. 1) showed the solid to be composed of small platelets ($\leq$0.5 μm in diameter) that coalesced to form bluntly terminated needles $\geq$4 μm in length. X-ray diffraction analysis showed the solid to be composed entirely of aragonite. Surface area of the seed was 2.41 m^2 gm^{-1} as determined by the Kr-BET method described by de Kanel and Morse (1979).

3 Methods

A temperature-controlled water bath was used to maintain aliquots of the stock solution at 10.0°, 25.0°, or 40.0° ± 0.2°C. pH measurements were made using a Leeds and Northrop 7415 Research pH Meter and a Metrohm combination glass electrode standardized with

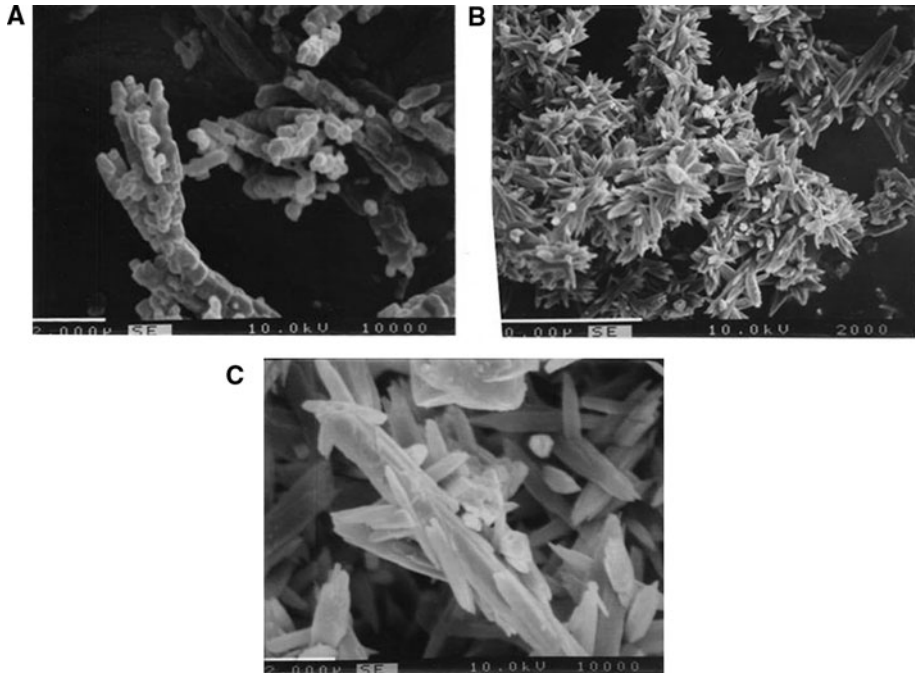

Fig. 1 SEM photomicrographs of **a** aragonite seed material; scale bar = 2.0 microns, and the final solid for run A255 at 25°C that contained 21.1 mg seed material and 79.9 mg of overgrowth: **b** scale bar = 10.0 microns and **c** Close up of B; *scale bar* = 2.0 microns

S/P Calibrated NBS Buffers. Total alkalinity measurements (A_T) were made using the Gran (1952) titration method to a precision of better than 0.7%. Calcium concentrations (T_{Ca}) were measured by complexiметric titration using EGTA to a precision of better than 0.4%.

3.1 Experimental Procedures

Prior to an experimental run, ~300 ml of stock solution was chemically reequilibrated with a CO_2/N_2 gas phase to create a solution supersaturated with respect to aragonite. This was accomplished by bubbling the water-saturated CO_2/N_2 gas mixture (300 ml min^{-1}) through a solution as it was stirred in a constant temperature vessel. Chemical reequilibration of the solution was monitored using a pH electrode and meter. One hour after the stabilization of pH, samples of the solution (~25 ml) were collected for total alkalinity (A_T) and calcium (T_{Ca}) analysis. Immediately after sampling, a known weight of aragonite seed material (20 to 30 mg) was added to the reaction vessel to initiate the heterogeneous growth of aragonite. The rate of titrant input was controlled with a peristaltic pump to maintain pH at a constant value throughout an experiment; adjustments in titrant flow rate were required within the first few minutes of some runs to stabilize pH. The mass of overgrowth was controlled by the chemistry and volume of titrants added. Upon completion of an experiment, samples of the final solution were collected in a syringe and filtered through a 0.4-μm polycarbonate filter for chemical analysis (as described earlier). The remaining solid and solution were immediately separated by filtration using a preweighed 0.45-μm polycarbonate filter. Methanol was used to remove any carbonate grains

that adhered to reaction system components. After filtering the methanol rinsate, the solid/filter was dried for ~10 h at 60°C and reweighed to provide a quantitative estimate of the carbonate yield.

Uncertainty in yield was quantified to estimate error in the calculation of precipitation. Preliminary recovery experiments (i.e., no precipitation) using seed material and carbonate-equilibrated water demonstrated that final seed weight did not vary from initial weight by more than 3 mg under simulated run conditions. Based on the mass of overgrowth precipitated in each run, the error associated with recovery was less than the change in precipitation rate during a run (as discussed elsewhere). For additional detail, see Romanek et al. (1992).

3.2 Solution PCO_2

Reequilibration of stock solution at lower PCO_2 increased the pH and $CO^{2-}_{3(aq)}$ content of the solution and reset the saturation state of the solution with respect to aragonite. Solution pH values were used in conjunction with initial total alkalinities to calculate the PCO_2 of the experimental solutions. Calculated PCO_2 values were compared with the PCO_2 of CO_2/N_2 tank gas mixtures measured by gas chromatography to ensure that chemical equilibrium was established prior to each experimental run.

3.3 Run Product Mineralogy

A preliminary check of the final run product mineralogy using standard X-ray diffraction techniques revealed that a small amount of calcite precipitated in some runs. The calcite component was quantified using a calibration curve relating the percentage of calcite in standard aragonite/calcite mixtures to the area ratio of the (104) calcite peak to the (021) and (111) aragonite peaks plus the (104) calcite peak. Because the intensity of the (104) peak for a randomly oriented sample of pure calcite is many times larger than the combined (021) and (111) peaks for a pure aragonite powder, this technique is highly sensitive to minor calcite admixtures. The linear dependence for the relationship observed in this study was similar to that reported by Davies and Hooper (1963). Using the empirical calibration curve, the mass of calcite was quantified and subtracted from the final weight measurement of each run before rate measurements were determined.

3.4 Calculation of Saturation State

The aqueous chemistry of the solution was modeled to determine the saturation state with respect to aragonite. Saturation state was calculated by dividing the ionic activity product (IAP), defined as $a(Ca^{2+}) \cdot a(CO_3^{2-})$, where $a = m(x)\gamma(x)$, and $m(x)$ = molarity and $\gamma(x)$ = activity coefficient, by the solubility product (K_{SP}) for the pure mineral (Morse and Mackenzie 1990). Activity coefficients were calculated from measurements of temperature, pH, aqueous Ca^{2+} concentration, and total alkalinity, while aqueous Na^+ and Cl^- concentration were estimated based on reagent stoichiometry. The Debye–Hückel equation was used to calculate free ion activity coefficients for all dissolved species, including all dissolved inorganic carbon species. Total activity coefficients were determined by adjusting free activity coefficients to account for the percentage of a species that exists in the form of ion pairs or complexes (e.g., $CaHCO_3^+$, $CaCO_3^\circ$, $NaHCO_3^\circ$, and $NaCO_3^-$). The temperature dependence for all association constants, equilibrium constants, and the

solubility product were considered when possible (Butler and Huston 1970; Plummer and Busenberg 1982; Nordstrom et al. 1990).

3.5 Calculation of Precipitation Rate

The precipitation rate for each run was calculated in the units of micromol m^{-2} h^{-1} using the following values: the initial weight of seed material, the final weight of the solid (seed plus overgrowth), the specific surface area of solid carbonate acting as a substrate for precipitation, and the duration of a run.

Previous studies showed that the precipitation rate of solid carbonate is governed by surface reactions and a term for surface area must be incorporated into a rate expression (e.g., Wiechers et al. 1975). Surface area of the final solid in each experiment was determined as a function of the percent overgrowth. Aragonite BET surface area measurements decreased linearly with percent overgrowth, from 2.41 m^2 gm^{-1} for seed material to 0.81 m^2 gm^{-1} for a 74% overgrowth ($r = 0.945$ for $N = 6$). Theoretical modeling of aragonite surface area using a right circular cone with a height-to-base diameter ratio of 5 matched the BET surface area measurements and the height-to-base diameter ratios measured from SEM images. The correspondence in observed and theoretical measurements suggests that potential modifications in surface roughness did not add a significant component to the final surface area of solid for each run.

Initial and final specific surface areas were calculated from the mass of the seed or final solid, the fraction of overgrowth, and the empirical curve relating percent overgrowth to surface area. Initial and final precipitation rates were determined from the bulk production rate (mass/time) normalized to the initial or final specific surface area for a run.

Using an invariant bulk production rate to calculate initial and final precipitation rate produces values which are functionally related by the ratio of final to initial specific surface area. Consequently, initial precipitation rate was always greater than final rate, with the difference increasing as the fraction of overgrowth increased. To accommodate these slight changes, all precipitation rate data are reported as initial, final, and average rates. The use of average values is meaningful because theoretical modeling and empirical results demonstrate that normalized surface area varies linearly with the fraction of overgrowth during a run.

The dominant components of uncertainty in the determination of precipitation rate are errors in BET surface area measurement and final solid weight measurements. These two sources of error account for less than 6% of the average rate value; generally, they are less than the change in rate during a run.

3.6 Saturation State–Precipitation Rate Relations

Previous work using the chemo-stat technique has shown that $CaCO_3$ precipitation rate is related to saturation state when solutions are held at a steady-state level of supersaturation (e.g., Mucci and Morse 1983). The most common form of the empirical equation used to model carbonate reaction kinetics is:

$$R = k(\Omega - 1)^n \tag{1}$$

where R is precipitation rate, k is rate constant, n is the empirical reaction order, and Ω is the saturation state of the solution for the relevant mineralogical phase. The logarithmic form of the equation is as follows:

$$\log R = \log k + n \log(\Omega - 1) \quad (2)$$

On a log R versus log $(\Omega - 1)$ plot, the slope of the trend in the data is the reaction order (n) and the y-intercept is the log of the rate constant (k).

The Arrhenius activation energy for the reaction may be determined from the equation:

$$\mathrm{k} = \mathrm{A}\,\mathrm{e}^{-\mathrm{E}}/\mathrm{RT} \quad (3)$$

where k is rate constant, A is a collisional frequency factor term, E is the activation energy, R is the gas constant, and T is temperature (e.g., Crassford et al. 1983). The activation energy may be determined from the slope of the logarithmic form of the equation:

$$\log k = \log A + (-E/R) \cdot (1/T) \quad (4)$$

4 Results

4.1 Bulk Chemistry

The initial and final bulk chemistry of individual runs is summarized in Table 1. Greater than 90% of the final Ca^{2+} and alkalinity (A_T) values were within ± 1 mmol l^{-1} and ± 2 meq l^{-1} of the initial values, respectively (Fig. 2). Changes in Ca^{2+} and A_T plot along a line having a slope of 1:2, which is compatible with the removal of these ions by the precipitation of a solid carbonate phase according to the charge balance consideration: $\Delta Ca^{2+} = 2\Delta A_T$. Within the uncertainty of the measurements, the observed final Ca^{2+} and A_T values were within 1% of the predicted values based on mass balance considerations using solution compositions, the mass of titrant input, and the weight of the final solid.

Experimental pH values ranged from 6.6 to 7.9, and solution PCO_2 values ranged between 0.0078 and 0.1785. During some of the runs, solution PCO_2 increased because of a self-titration effect. Initial ionic strength (I) ranged from 0.05 to 0.07 mol l^{-1} (Table 2), and it did not vary significantly throughout an experimental run.

4.2 Precipitation Kinetics

Initial, final, and average saturation state and precipitation rate for individual runs are reported in Table 2. The range of average saturation states was 8.3 to 28.5 at 10°C, 2.9 to 19.6 at 25°C, and 2.0 to 10.0 at 40°C, and the range of average precipitation rates was $10^{2.8}$ to $10^{3.8}$ micromol m^{-2} h^{-1} at 10°C, $10^{2.3}$ to $10^{4.0}$ micromol m^{-2} h^{-1} at 25°C, and $10^{2.5}$ to $10^{4.1}$ micromol m^{-2} h^{-1} at 40°C.

The relationship between saturation state and precipitation rate was determined using average saturation state [log $(\Omega - 1)$] and precipitation rate (log R) values for each run; the data are presented for each temperature in Fig. 3. A linear regression model that incorporates error in the both variables (York 1966) was used to calculate an equation for the best-fit line of each data suite to determine reaction orders, rate constants, and their associated errors. Initial, final, and average reaction orders and rate constants are reported in Table 3. Saturation state is positively correlated with precipitation rate at each temperature, and average correlation coefficients are all greater than 0.972. Lower temperature runs required higher relative saturation states to maintain a constant precipitation rate. Average reaction orders were 1.74 ± 0.10, 1.74 ± 0.07, and 1.52 ± 0.06 at 10°, 25°, and 40°C, respectively. The slight decrease in reaction order with temperature is not

Table 1 Initial and final values of bulk chemistry for experimental runs

Run #	Temp. (°C)	pH (i)‡	pH (f)‡	PCO_2‡‡ (i)	PCO_2 (f)	Alk* (i)	Alk (f)	Ca^{2+} (i)	Ca^{2+} (f)	Na^+ (i)	Na^+ (f)	Cl^- (i)	Cl^- (f)
A265	10	7.31	7.41	0.0302	0.0245	15.07	15.38	15.30	15.10	15.1	18.0	30.6	33.0
A266	10	7.28	7.38	0.0318	0.0254	14.90	14.83	15.29	14.99	14.9	17.9	30.6	32.9
A267	10	7.30	7.28	0.0310	0.0311	15.12	14.45	15.30	14.81	15.1	17.9	30.6	32.7
A272	10	7.85	7.73	0.0088	0.0125	15.29	16.68	15.31	16.09	15.3	17.9	30.6	33.0
A273	10	7.81	7.72	0.0094	0.0116	14.97	14.96	15.20	15.19	15.0	17.9	30.4	32.8
A274	10	7.83	7.73	0.0090	0.0113	14.88	15.27	15.46	15.53	14.9	17.8	30.9	33.1
A275	10	7.66	7.67	0.0090	0.0094	10.10	10.75	15.08	15.50	10.1	12.9	30.2	32.6
A276	10	7.67	7.72	0.0089	0.0078	10.03	9.98	15.20	15.07	10.0	12.9	30.4	32.8
A277	10	7.67	7.72	0.0089	0.0081	10.28	10.49	15.13	15.15	10.3	13.1	30.3	32.8
A281	10	7.78	7.69	0.0103	0.0092	15.11	11.15	15.04	13.52	15.1	17.7	30.1	32.3
A282	10	7.68	7.68	0.0113	0.0106	13.19	12.64	15.08	14.53	13.2	16.8	30.2	33.8
A283	10	7.68	7.70	0.0111	0.0104	13.18	12.86	15.09	14.63	13.2	16.9	30.2	33.6
A284	10	7.72	7.73	0.0104	0.0100	13.29	13.23	15.32	15.14	13.3	16.9	30.6	33.7
A226	25	6.83	6.82	0.1090	0.1258	14.62	17.17	15.00	16.38	14.6	17.7	30.0	32.5
A227	25	6.82	6.83	0.1114	0.1223	15.00	17.06	15.12	16.16	15.0	18.0	30.2	32.7
A228	25	6.85	6.83	0.1056	0.1196	15.23	16.64	14.99	15.79	15.2	18.3	30.0	32.6
A230	25	6.69	6.68	0.1039	0.1553	10.28	15.29	14.92	16.23	10.3	15.5	29.8	32.4
A231	25	6.72	6.69	0.0960	0.1550	10.21	15.68	15.23	16.68	10.2	15.9	30.5	33.0
A232	25	6.67	6.63	0.1079	0.1785	10.21	15.89	15.11	16.46	10.2	16.4	30.2	33.1
A233	25	6.95	7.05	0.0849	0.0630	15.41	14.53	14.92	14.12	15.4	18.2	29.8	31.9
A234	25	7.02	7.01	0.0721	0.0706	15.38	14.73	14.90	14.57	15.4	18.2	29.8	32.1
A235	25	7.03	6.99	0.0708	0.0719	15.44	14.98	14.87	14.28	15.4	18.4	29.7	32.3
A236	25	7.02	7.00	0.0714	0.0717	15.41	14.59	14.97	14.36	15.4	18.3	29.9	32.4
A244	25	7.15	7.15	0.0520	0.0544	15.00	15.74	14.89	15.02	15.0	18.1	29.8	32.4
A245	25	7.17	7.17	0.0494	0.0500	15.15	15.13	15.00	14.92	15.2	18.2	30.0	32.6
A246	25	7.18	7.16	0.0487	0.0519	15.03	15.48	14.94	15.03	15.0	18.2	29.9	32.5
A247	25	7.45	7.41	0.0261	0.0311	15.00	16.63	14.96	15.80	15.0	18.0	29.9	32.6
A252	25	7.43	7.34	0.0268	0.0321	14.91	14.64	15.08	16.00	14.9	15.5	30.2	32.6
A253	25	7.29	7.29	0.0258	0.0284	10.34	11.45	15.28	15.74	10.3	13.2	30.6	32.9
A254	25	7.29	7.31	0.0257	0.0291	10.33	12.21	15.26	15.94	10.3	13.2	30.5	33.1
A255	25	7.31	7.27	0.0245	0.0260	10.28	10.02	15.23	14.98	10.3	12.9	30.5	32.8
A259	25	7.28	7.30	0.0379	0.0390	14.94	16.04	15.21	15.85	14.9	18.1	30.4	32.8
A260	25	7.29	7.28	0.0377	0.0403	15.02	15.92	15.28	15.55	15.0	18.1	30.6	32.9
A261	25	7.32	7.28	0.0352	0.0387	15.25	15.10	15.42	15.06	15.3	17.8	30.8	33.1
A214	40	6.79	6.82	0.1163	0.1124	11.15	11.57	5.57	5.55	34.1	35.1	34.1	34.9
A215	40	6.80	6.83	0.1157	0.1096	11.36	11.54	5.57	5.49	34.4	35.2	34.1	34.9
A216	40	6.76	6.76	0.1248	0.1258	11.17	11.27	5.59	5.52	34.2	34.9	34.2	35.1
A217	40	6.74	6.75	0.1122	0.1017	10.16	9.43	15.11	14.86	10.2	12.0	30.2	32.7
A218	40	6.76	6.76	0.1065	0.1024	10.10	9.70	15.12	14.69	10.1	12.3	30.2	32.1
A219	40	6.77	6.79	0.1047	0.0983	10.17	10.00	15.17	14.89	10.2	12.5	30.3	32.2
A223	40	6.97	6.97	0.0972	0.0957	15.05	14.67	15.00	14.83	15.1	18.1	30.0	32.5

Table 1 continued

Run #	Temp. (°C)	pH (i)‡	pH (f)‡	PCO_2‡‡ (i)	PCO_2 (f)	Alk* (i)	Alk (f)	Ca^{2+} (i)	Ca^{2+} (f)	Na^+ (i)	Na^+ (f)	Cl^- (i)	Cl^- (f)
A224	40	7.01	7.00	0.0892	0.0893	15.00	14.90	15.31	15.23	15.0	17.9	30.6	32.8
A225	40	6.97	6.96	0.0969	0.0988	13.19	15.12	15.00	16.03	13.2	17.1	30.0	32.3

All units are in mmol l^{-1}, except for alkalinity (alk), which is reported in the units of meq l^{-1}

‡ i initial, f final value

‡‡ PCO_2 calculated from total alkalinity (A_T) and pH at beginning and end of run

* Total alkalinity as measured by Gran titration

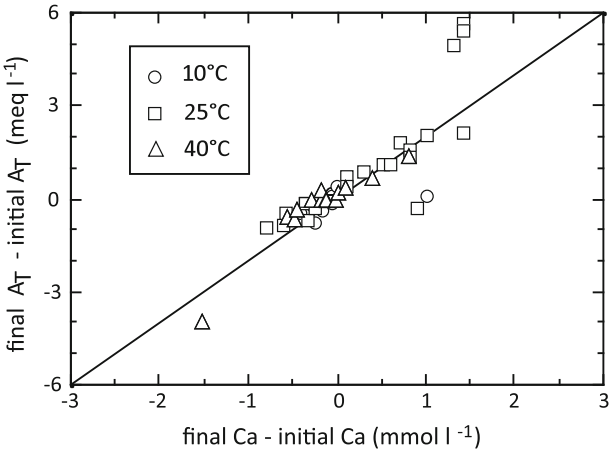

Fig. 2 Difference between final and initial aqueous Ca^{2+} and total alkalinity (and A_T) values for each experimental run. Solid line is 2:1 slope through the origin. If solution chemistry remained invariant throughout an experiment, differences in Ca^{2+} and A_T would plot at the origin. The departure of data from the origin along the 2:1 line is consistent with the establishment of an invariant state of supersaturation as aragonite precipitation rate and titrant input reach steady-state conditions. Significant displacement off the 2:1 line occurred in a few runs because of the inadvertent use of a titrant/solution combination that did not contain an excess ion concentration of A_T: Ca^{2+} in a 2:1 ratio

statistically significant. Average rate constants were $10^{1.27} \pm 0.12$, $10^{1.85} \pm 0.06$, and $10^{2.55} \pm 0.04$ micromol m^{-2} h^{-1} at 10°, 25°, and 40°C; they are strongly temperature dependent, increasing one-half order of magnitude for each 15°C rise in temperature. Using these data in Eqs. 3 and 4, an Arrhenius activation energy of 71.2 kJ mol^{-1} is calculated for the heterogeneous precipitation of aragonite from dilute solutions.

5 Discussion

Most experimental studies of the reaction kinetics of carbonate minerals in dilute solution utilize the free-drift (e.g., Reddy and Nancollas 1971; Nancollas and Reddy 1971) or pH-stat technique (e.g., Morse 1974) in which the solution chemistry drifts during the experiment. Busenberg and Plummer (1986), Walter (1986), and Burton (1988) provide the only data on aragonite precipitation kinetics using a chemo-stat technique in which the

Table 2 Temperature and initial and final values of ionic strength, saturation state, and precipitation rate for experimental runs

Run #	Temp. (°C)	Time (min)	Ionic strength		Log ($\Omega - 1$)			Log rate[‡‡]		
			(i)[‡]	(f)[‡]	(i)	(f)	(avg)[†]	(i)	(f)	(avg)
A265	10	526	0.061	0.064	0.90	1.01	0.96	3.00	2.80	2.91
A266	10	549	0.061	0.063	0.86	0.95	0.91	2.93	2.75	2.85
A267	10	621	0.061	0.062	0.89	0.83	0.86	2.92	2.73	2.84
A272	10	56	0.062	0.066	1.47	1.40	1.44	3.88	3.71	3.81
A273	10	133	0.061	0.064	1.43	1.32	1.38	3.80	3.52	3.68
A274	10	108	0.062	0.065	1.45	1.36	1.40	3.85	3.59	3.74
A275	10	209	0.056	0.059	1.11	1.15	1.13	3.45	3.23	3.35
A276	10	315	0.056	0.058	1.12	1.16	1.14	3.34	3.10	3.24
A277	10	277	0.056	0.059	1.14	1.19	1.16	3.35	3.13	3.25
A281	10	460	0.061	0.058	1.39	1.14	1.27	3.49	3.11	3.34
A282	10	298	0.059	0.061	1.24	1.21	1.22	3.49	3.20	3.37
A283	10	271	0.059	0.061	1.25	1.23	1.24	3.57	3.26	3.44
A284	10	224	0.060	0.063	1.29	1.29	1.29	3.62	3.33	3.50
A226	25	203	0.060	0.067	0.57	0.65	0.61	2.97	2.87	2.92
A227	25	240	0.060	0.066	0.57	0.65	0.61	2.97	2.86	2.91
A228	25	308	0.060	0.065	0.60	0.63	0.62	2.89	2.78	2.84
A230	25	480	0.055	0.064	0.18	0.41	0.31	2.28	2.22	2.25
A231	25	517	0.056	0.066	0.23	0.45	0.34	2.44	2.36	2.40
A232	25	307	0.056	0.066	0.15	0.38	0.28	2.72	2.63	2.67
A233	25	368	0.060	0.061	0.72	0.79	0.76	3.32	3.06	3.21
A234	25	360	0.060	0.062	0.81	0.76	0.78	3.33	3.07	3.22
A235	25	407	0.060	0.062	0.82	0.76	0.79	3.30	3.03	3.18
A236	25	327	0.060	0.061	0.82	0.74	0.78	3.29	3.06	3.19
A244	25	143	0.060	0.063	0.94	0.96	0.95	3.65	3.43	3.55
A245	25	146	0.060	0.063	0.98	0.96	0.97	3.64	3.42	3.54
A246	25	170	0.060	0.063	0.98	0.97	0.97	3.64	3.39	3.54
A247	25	30	0.060	0.066	1.26	1.28	1.27	4.08	3.93	4.01
A252	25	23	0.060	0.064	1.25	1.17	1.21	4.05	3.93	4.00
A253	25	97	0.056	0.060	0.96	1.01	0.98	3.72	3.53	3.63
A254	25	69	0.056	0.061	0.96	1.06	1.01	3.68	3.54	3.62
A255	25	164	0.056	0.058	0.98	0.91	0.95	3.69	3.42	3.58
A259	25	61	0.061	0.065	1.10	1.15	1.12	3.89	3.71	3.81
A260	25	81	0.061	0.065	1.10	1.12	1.11	3.85	3.64	3.76
A261	25	99	0.062	0.063	1.15	1.09	1.12	3.84	3.60	3.74
A214	40	309	0.051	0.052	0.04	0.11	0.08	2.69	2.61	2.65
A215	40	388	0.051	0.052	0.08	0.15	0.11	2.68	2.58	2.63
A216	40	531	0.051	0.052	0.00	0.00	0.00	2.59	2.49	2.54
A217	40	106	0.056	0.057	0.53	0.49	0.51	3.47	3.33	3.41
A218	40	79	0.056	0.057	0.56	0.52	0.54	3.53	3.38	3.46
A219	40	123	0.056	0.057	0.57	0.58	0.57	3.52	3.35	3.44

Table 2 continued

Run #	Temp. (°C)	Time (min)	Ionic strength		Log (Ω − 1)			Log rate‡‡		
			(i)‡	(f)‡	(i)	(f)	(avg)†	(i)	(f)	(avg)
A223	40	66	0.060	0.062	0.97	0.94	0.96	4.08	3.82	3.97
A224	40	59	0.061	0.063	1.01	1.00	1.00	4.17	3.89	4.05
A225	40	65	0.060	0.065	0.90	0.98	0.94	4.05	3.80	3.94

‡ *i* initial, *f* final value

‡‡ Rate constants are reported in log units of micromol m^{-2} h^{-1}

† Average of i and f values

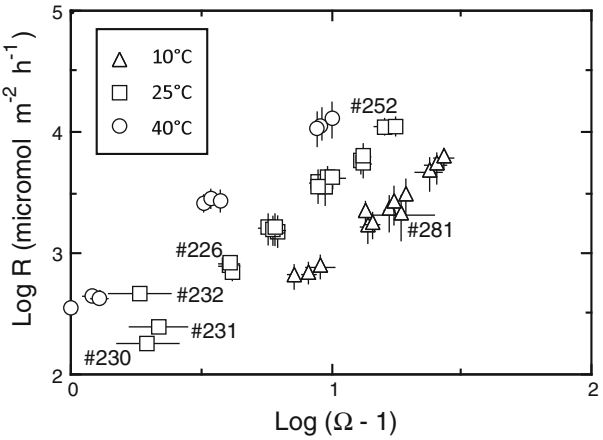

Fig. 3 Precipitation rate (R) in log units of micromol m^{-2} h^{-1} as a function of saturation state in log (Ω − 1) units for each run of this study. Calculation of R and Ω is described in the text. The termination of *horizontal* and *vertical lines* passing through each symbol represents the initial and final precipitation rate and saturation state for each run. Where they are not present, the range in values is less than the size of the symbol. Best-fit lines are regressions using the model by York (1966). Runs in which solution chemistry changed by greater than ±1 mmol l^{-1} Ca^{2+} or ±2 meq l^{-1} A_T are labeled to show that they conform to the trends displayed by the remaining data

Table 3 Calculated reaction orders (n) and rate constants‡ (k) from saturation state–precipitation rate relations of experimental runs using linear regression model incorporating error in both variables (York 1966)

Mineralogy	T (°C)	Reaction order (*n*)			Rate constant (Log *k*)‡			*n**
		(i)‡‡	(f)‡‡	(avg)‡‡	(i)	(f)	(avg)	
Aragonite	10	1.55 ± 0.13	1.90 ± 0.16	1.74 ± 0.10	1.58 ± 0.16	0.96 ± 0.19	1.27 ± 0.12	13
Aragonite	25	1.60 ± 0.08	1.83 ± 0.08	1.74 ± 0.07	2.08 ± 0.07	1.65 ± 0.07	1.85 ± 0.06	21
Aragonite	40	1.59 ± 0.03	1.42 ± 0.09	1.52 ± 0.06	2.61 ± 0.02	2.50 ± 0.06	2.55 ± 0.04	9

‡ All rate constants are in log units of micromol m^{-2} h^{-1}

‡‡ (i) initial, (f) final, (avg) average

* *n* number of observations

aqueous chemistry is fixed, and PCO_2 is maintained by bubbling; their experiments were conducted only at 25°C. In their studies, precipitation rate was primarily determined by the addition rate and concentration of titrants added during the precipitation reaction. In this study, however, rate was calculated directly by the mass of solid precipitated per unit time, taking into consideration the change in surface area over the course of the run. A comparison of precipitation rates computed by these two independent methods for this study revealed they were within 1% of each other. Heretofore, all precipitation rates are reported on a mass basis.

5.1 Comparison With Previous Studies at 25°C

Although the kinetic data fall within distinct fields, the trends are internally consistent and similar to previous studies (Fig. 4). Differences may be attributed to analytical factors such as the choice of models and/or method(s) used to calculate saturation state or precipitation rate, or they may be related to distinct methodological aspects of the studies, e.g., such as the choice of solution PCO_2 for a particular set of experiments. To test the former hypothesis, the saturation state data from Burton (1988) were recalculated using the ion speciation model of this study. Despite the potential confounding influence of solution PCO_2 (3 to 14% for this study and 1.0% for Burton), the recalculated data from Burton are nearly identical to our data, with a reaction order and rate constant of 1.99 ± 0.10 and $10^{1.45} \pm 0.32$ micromol m^{-2} h^{-1}, respectively.

While kinetic data from Busenberg and Plummer (1986) are included in Fig. 4 for comparison, solution chemistries were not reported in sufficient detail to recalculate saturation state for this study. Nevertheless, their data provide significant insight into the potential effect of PCO_2 on aragonite precipitation kinetics because they showed that precipitation rate increases at a constant saturation state as PCO_2 increases over a wide range of values (0.03 to 96% CO_2). Their data at the lowest PCO_2 (0.03 to 10%) are most similar to the kinetic data of this study and the recalculated data from Burton. It is probable

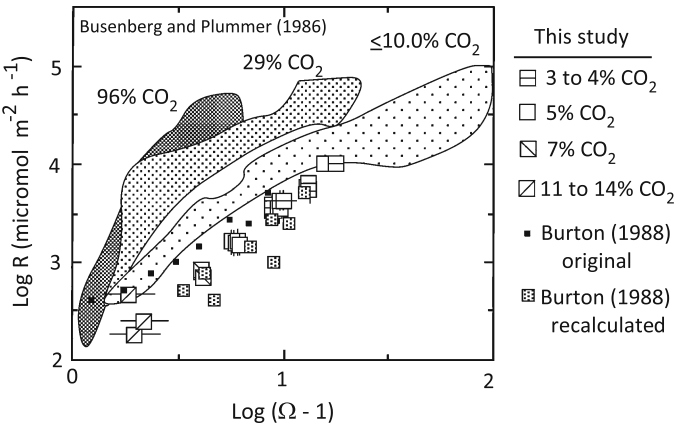

Fig. 4 Log R versus log $(\Omega - 1)$ values of this study compared with other dilute solution data at 25°C. Saturation states from Burton (1988) were recast using the Debye–Huckel ion speciation model used in this study (as described in the text). The data from Burton are for a solution PCO_2 of 1.0%. Saturation states were not recalculated from the data by Busenberg and Plummer (1986) because of insufficient detail in solution chemistry. *Error bars* are the same as described in Fig. 3

that a PCO_2 effect is expressed in our data as well but the magnitude of the effect is small over the limited range of PCO_2 investigated.

In addition to these factors, differences in precipitation rates may be caused by the homogeneous or secondary nucleation of aragonite (deBoer 1977) during our experiments, but scanning electron photomicrographs of the final solid from several of our runs revealed little evidence for variability in grain size. Alternatively, differences in dislocation densities of seed material may account for differences in precipitation rate (Crassford et al. 1983) but these data are rarely, if ever, reported in studies of carbonate precipitation kinetics.

Finally, differences in solid/solution ratio can also cause variations in precipitation rate. Reddy and Gaillard (1981) showed that solid/solution ratio covaries negatively with rate constant below a ratio of about 300 mg l^{-1}, whereas between 300 and 2,500 mg l^{-1} rate constant does not vary. These differences are attributed to the formation of new nuclei on solid surfaces at relatively low solid/solution ratio while surface growth is facilitated at relatively high solid/solution ratio. The average solid/solution ratio for individual runs of this study ranged from 70 to 150 mg l^{-1}, while Burton's ratios ranged from about 10 to 60 mg l^{-1}. The similarity in precipitation kinetics (i.e., rate constant) for these two studies contrasts with the twofold change in rate constant observed by Reddy and Gaillard over a similar range in solid/solution ratio, suggesting that surface growth is the primary mode of crystal growth in the present study. The discrepancy with the results by Reddy and Gaillard (1981) and Busenberg and Plummer (1986) may result from differences in solution chemistry as the potential exists for nucleation and surface growth effects to be expressed at constant solid/solution ratio over a broad range in solution supersaturation states.

5.2 Comparison with Precipitation Kinetics in Seawater

Results from this study are also compared with previous studies using natural and artificial seawater to document the effect of aqueous constituents and ionic strength on aragonite precipitation kinetics (Figs. 5 through 7; Table 4). No attempt was made to recalculate seawater saturation state using the Debye–Hückel equation due to inadequacies of this model at ionic strengths greater than 0.1 mol l^{-1} (Morse and Mackenzie 1990). Nevertheless, reaction orders and rate constants were recalculated from the original data using the linear regression model of York (1966) to generate estimates of error for these parameters. For this analysis, uncertainty in precipitation rate was estimated at $\pm 15\%$ based on the percentage of overgrowth generated in these studies, while error in saturation state was estimated at $\pm 5\%$.

5.2.1 Precipitation Kinetics at 5° to 10°C

Precipitation rate increases systematically with saturation state for the dilute solution data of this study at 10°C, while precipitation rate in seawater (Burton 1988) is nearly insensitive to changes in saturation state at 5°C (Fig. 5). The present study shows a trend which is internally consistent despite a tenfold change in solution PCO_2, suggesting that relatively small differences in solution PCO_2 do not affect precipitation rate appreciably at relatively low temperature. Differences in precipitation rate between the two studies may be explained in part by differences in solid/solution ratio since the ratios for this study (93 to 193 mg l^{-1}) are significantly lower than those in seawater (400 to 1,200 mg l^{-1}). Alternatively, aqueous SO_4^{2-} in seawater may have suppressed precipitation rates for aragonite.

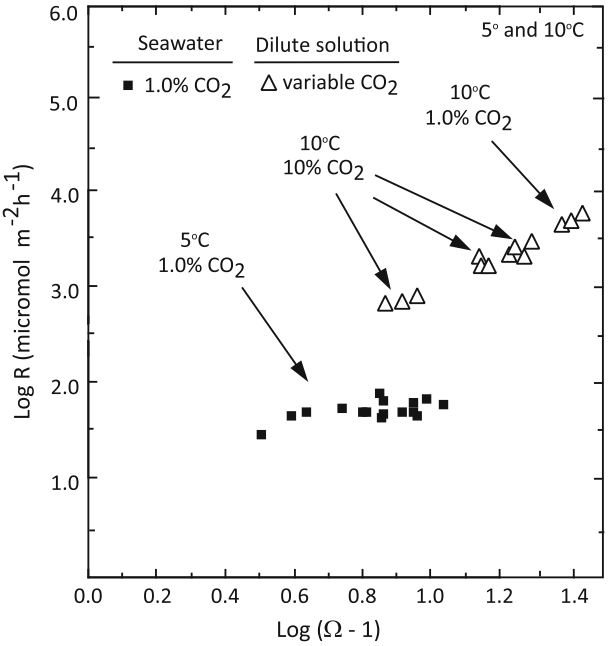

Fig. 5 Log R versus log ($\Omega - 1$) values for 10°C aragonite runs of this study (*open triangles*) and data (*filled squares*) from Burton (1988) at 5°C. Solution PCO_2 values are as indicated in figure. *Error bars* are the same as described in Fig. 3

Table 4 Reaction orders and rate constants for published data in artificial and natural seawater studies

Temp. (°C)	Reaction order	Rate constant‡‡	PCO_2 (%)	Solution (n or a)‡	Solid/solution ratio (mg L^{-1})	Reference
5°	0.4 ± 0.1*	1.34 ± 0.11*	1.0	n	400–1,200	Burton (1988)
25°	2.86 ± 0.11	0.43 ± 0.31	0.03	n	60–100	Burton (1988)
	1.70 ± 0.16	1.61 ± 0.04	1.0	n	22–400	Burton (1988)
	2.22 ± 0.18	1.33 ± 0.53	10.0	n	100–800	Burton (1988)
	1.53 ± 0.12	1.42 ± 0.05	0.3	a	500–2,000	Mucci et al. (1989)
	1.19 ± 0.12	2.22 ± 0.08	1.0	a	100–200	Burton (1988)
	2.55 ± 0.15	1.48 ± 0.33	0.3	a (SO_4-free)	500–2,000	Mucci et al. (1989)
37°	2.49 ± 0.17	1.61 ± 0.10	1.0	n	30–200	Burton (1988)

‡ n natural seawater, a artificial seawater

‡‡ Rate constants are reported in log units of micromol m^{-2} h^{-1}

* Value quoted from Burton and Walter (1987)

5.2.2 Precipitation Kinetics at 25°C

The dilute solution data of this study are similar to data from natural and artificial seawater (Fig. 6). The seawater data show a slight tendency for increased precipitation rate at higher solution PCO_2 for a given saturation state, but variability in the data is too great to establish

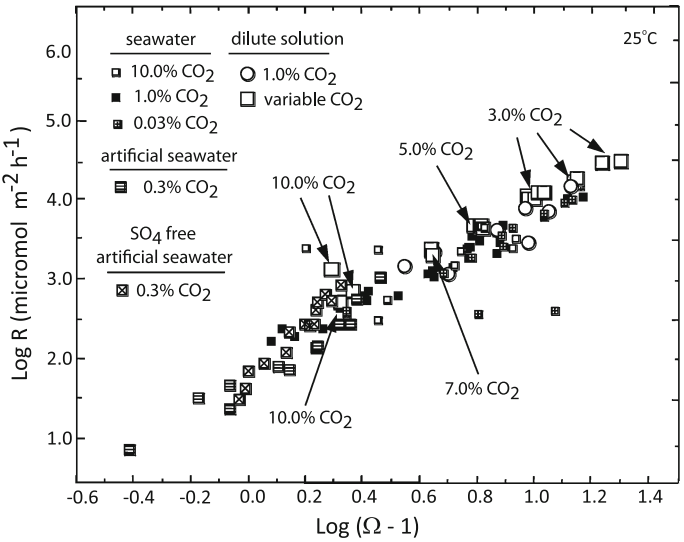

Fig. 6 Log R versus log ($\Omega - 1$) values for 25°C aragonite runs of this study (*large open squares* and *circles*) compared with natural seawater data from Burton (1988: *various small squares*), artificial seawater from Mucci et al. (1989: *intermediate size squares with horizontal lines*), and SO_4-free artificial seawater from Mucci et al. (1989: *intermediate squares* with "x"s). *Error bars* are the same as in Fig. 3. Solution PCO_2 values are as indicated in the figure

this relationship with statistical certainty. Reaction orders and rate constants for natural seawater data (Burton 1988), artificial seawater data (Burton 1988; Mucci et al. 1989), and SO_4-free artificial seawater data (Mucci et al. 1989) are similar to values in dilute solution and show no dependence on solution PCO_2 for a range of values between 0.03 and 10.0% (Table 4). Reaction order is highest and rate constant is lowest for the 0.03% solution PCO_2 data from Burton, but the values are strongly influenced by two data points with anomalously low precipitation rates. The similarity of the dilute solution data (with solid/solution ratios from 10 to 150 mg l^{-1}) and the natural and artificial seawater data (with ratios from 22 to 2,000 mg l^{-1}) suggests that solid/solution ratio does not affect aragonite precipitation rate over a large range of ratios at intermediate temperature. Differences in solution chemistry do not appear to affect precipitation rate over most of the range of saturation states investigated, while at relatively low saturation states Mucci et al. (1989) showed that SO_4^{2-} reduces the precipitation rate of aragonite when it is added to artificial seawater.

5.2.3 Precipitation Kinetics at 37° and 40°C

At $\log(\Omega - 1)$ values near 1.0, the dilute solution data of this study are similar to those in natural seawater at 37°C (Burton 1988) despite having solution PCO_2 values that differ by at least 8%, while at lower saturation states the dilute solution data have higher precipitation rates (Fig. 7). The trend for the data of this study is internally consistent over a 4% range in solution PCO_2, suggesting that changes in PCO_2 of this magnitude do not affect precipitation rate in dilute solutions at relatively high temperature, although the increase in

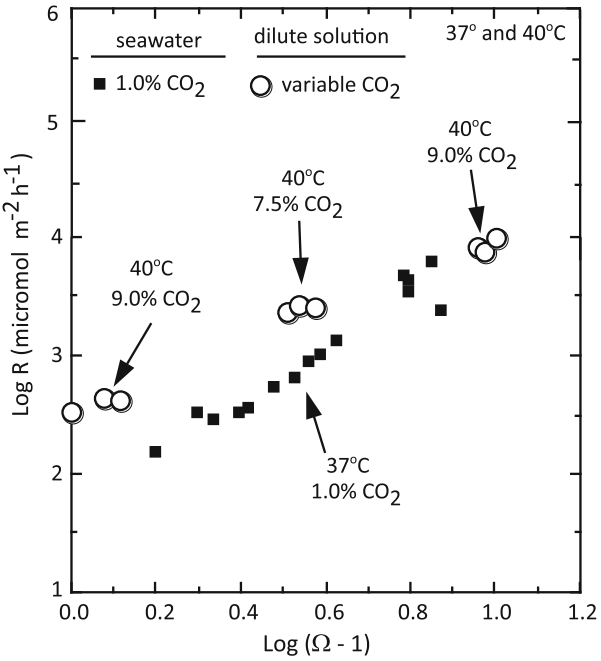

Fig. 7 Log R versus log ($\Omega - 1$) values for 40°C aragonite runs of this study (*open circles*) and natural seawater (*filled squares*) from Burton (1988) at 37°C. *Error bars* are the same as in Fig. 3. Solution PCO_2 values are as indicated in the figure

rate at relatively low saturation state is consistent with the PCO_2 effect observed by Busenberg and Plummer (1986). This is also consistent with Reddy et al. (1981) who found that the effect of solution PCO_2 is best expressed at low (but also high) saturation states. Average solid/solution ratios for this study ranged from 91 to 141 mg l^{-1} and are similar to those of Burton's seawater data (30 to 200 mg l^{-1}), so solid/solution ratio cannot explain variations in rate at low saturation states. Alternatively, SO_4^{2-} may inhibit precipitation rate as log($\Omega - 1$) values decrease, but the results by Mucci et al. (1989) at 25°C suggest an opposite effect. Unequivocal explanations for the difference in precipitation rate at 40°C cannot be determined at the present time.

5.3 Activation Energy for Aragonite

Finally, the data from this study were used to calculate an activation energy of 71.2 kJ mol^{-1} for the heterogeneous growth of aragonite. Only one other study has characterized the activation energy for aragonite. Munemoto and Fukushi (2008) reported a value of 80.7 kJ mol^{-1} for the transformation of Mg-bearing monohydrocalcite to aragonite through a dissolution–recrystallization mechanism over a temperature range of 10° to 50°C. Because these two studies differ in such fundamental ways, the activation energies may describe intrinsically different reaction mechanisms, although the similarity of values is striking.

Acknowledgments This project could not have succeeded without John Morse's thoughtful guidance and mastery of carbonate experimental systems. The writing is posthumous, but the science is a product of his mentorship and enthusiasm for carbonate geochemistry. This work was supported financially by the National Science Foundation (EAR-851187) and the NASA Astrobiology Institute.

References

Amjad Z (1987) Kinetic study of the seeded growth of calcium carbonate in the presence of benzene-polycarboxylic acids. Langmuir 3:224–228

Arnorsson S (1979) Hydrochemistry in geothermal investigations in Iceland techniques and applications. Nordic Hydrol 10:191–224

Berner RA, Westrich JT, Graber R, Smith J, Martens CS (1978) Inhibition of aragonite precipitation from supersaturated seawater; a laboratory and field study. Am J Sci 278:816–837

Burton EA (1988) Laboratory investigation of the effects of seawater chemistry on carbonate mineralogy. Ph.D. dissertation, Washington University, St. Louis MO, 306 pp

Burton EA, Walter LM (1987) Relative precipitation rates of aragonite and Mg calcite from seawater—temperature or carbonate ion control. Geology 15:111–114

Busenberg E, Plummer LN (1986) A comparative study of the dissolution and crystal growth kinetics of calcite and aragonite. In: Mumpton FA (ed) Studies in diagenesis. US Geol Surv Bull 1578:139–168

Butler JN, Huston R (1970) Activity coefficients and ion pairs in the systems sodium chloride-sodium bicarbonate-water and sodium chloride-sodium carbonate-water. J Phys Chem 74:2976–2983

Crassford GE, House WA, Pethybridge AD (1983) Crystallization kinetics of calcite from calcium bicarbonate solutions between 278.15 and 303.15 K. J Chem Soc Faraday Trans I 79:1617–1632

Davies TT, Hooper PR (1963) The determination of the calcite:aragonite ratio in mollusc shells by X-ray diffraction. Mineralog Mag 262:608–612

deBoer RB (1977) Influence of seed crystals on the precipitation of calcite and aragonite. Am J Sci 277:38–60

deKanel J, Morse JW (1979) A simple technique for surface area determination. J Phys E Sci Instr 12:272–273

Elfil H, Roques H (2004) Prediction of the limit of the metastable zone in the "CaCO3-CO2–H2O" system. Am Inst Chem Eng J 50:1908–1916

Elliot MN (1969) Present state of scale control in seawater evaporators. Desalination 6:87–104

Gran G (1952) Determination of the equivalence point in potentiometric titrations: part II. Analyst 77:661–671

Hu ZS, Deng YL (2003) Supersaturation control in aragonite synthesis using sparingly soluble calcium sulfate as reactants. J Colloid Interface Sci 266:359–365

Hu Z, Deng Y (2004) Synthesis of needle-like aragonite from calcium chloride and sparingly soluble magnesium carbonate. Powder Technol 140:10–16

Kawano J, Shimobayashi N, Miyake A, Kitamura M (2009) Precipitation diagram of calcium carbonate polymorphs: its construction and significance. J Phys Condens Matter 21:425102 (6 pp)

Kazmierczak TF, Tomson MB, Nancollas GH (1982) Crystal growth of calcium carbonate. A controlled composition kinetic study. J Phys Chem 86:103–107

Lee Y-J, Morse JW (1999) Calcite precipitation in synthetic veins: implications for the time and fluid volume necessary for vein filling. Chem Geol 156:151–170

Morse JW (1974) Dissolution kinetics of calcium carbonate in seawater 3. New method for study of carbonate reaction kinetics. Am J Sci 274:97–107

Morse JW, Berner RA (1972) Dissolution kinetics of calcium carbonate in seawater. 2. Kinetic origin for the lysocline. Am J Sci 272:840–851

Morse JW, Mackenzie FT (1990) Geochemistry of sedimentary carbonates. Developments in sedimentology 48. Elsevier, Amsterdam, p 707

Morse JW, Mackenzie FT (1993) Geochemical constraints on $CaCO_3$ transport in subsurface sedimentary environments. Chem Geol 105:181–196

Morse JW, deKanel J, Craig HL Jr (1979) A literature review of the saturation state of seawater with respect to calcium carbonate and its possible significance for scale formation on OTEC heat exchangers. Ocean Eng 6:297–315

Morse JW, Hanor JS, He S (1997) The role of mixing and migration of basinal waters in calcium carbonate mass transport. In: Monannes IP, Gregg JM, Shelton KL (eds) Basinwide fluid flow and associated diagenetic patterns: integrated petrologic, geochemical and hydrologic considerations. SEPM Special Publication No. 57. SEPM, Tulsa, pp 41–52

Morse JW, Andersson AJ, Mackenzie FT (2006) Initial responses of carbonate-rich shelf sediments to rising atmospheric pCO(2) and "ocean acidification": role of high Mg-calcites. Geochim Cosmochim Acta 70:5814–5830

Mucci A, Morse JW (1983) The incorporation of Mg^{2+} and Sr^{2+} into calcite overgrowths: influences of growth rate and solution composition. Geochim Cosmochim Acta 47:217–233

Mucci A, Morse JW (1990) Chemistry of low-temperature abiotic calcites: experimental studies on coprecipitation, stability, and fractionation. Rev Aquatic Sci 3:217–254
Mucci A, Canuel R, Zhong S (1989) The solubility of calcite and aragonite in sulfate-free seawater and the seeded growth kinetics and composition of the precipitates at 25°C. Chem Geol 74:309–320
Munemoto T, Fukushi K (2008) Transformation kinetics of monohydrocalcite to aragonite in aqueous solutions. J Mineral Petrol Sci 103:345–349
Nancollas GH, Reddy MM (1971) The crystallization of calcium carbonate II. Calcite growth mechanism. J Colloid Interface Sci 37:824–830
Nordstrom DK, Plummer LN, Langmuir D, Busenberg E, May HM, Jones BF, Parkhurst DL (1990) Revised chemical equilibrium data for major water-mineral reactions and their limitations. In: Bassett DC, Melchior RL (eds) Chemical modeling of aqueous systems II. American Chemical Society, Washington DC, pp 398–413
Omar W, Chen J, Ulrich J (2009) Application of seeded batch crystallization methods for reduction of the scaling tendency of seawater-a study of growth kinetics of calcium carbonate in seawater. Cryst Res Technol 44:469–476
Oudadesse H, Martin S, Derrien AC, Lucas-Girot A, Cathelineau G, Blondiaux G (2004) Determination of Ca, P, Sr and Mg in the synthetic biomaterial aragonite by NAA. J Radioanalyt Nuclear Chem 262:479–483
Packter AJ (1968) The precipitation of sparingly soluble alkaline-earth metal and lead salts: nucleation and growth orders during the induction period. J Chem Soc (A):859–862
Plummer LN, Busenberg E (1982) The solubilities of calcite, aragonite, and vaterite in CO_2–H_2O solutions between 0 and 90°C and an evaluation of the aqueous model for the system $CaCO_3$-CO_2–H_2O. Geochim Cosmochim Acta 46:1011–1040
Reddy MM (1978) Kinetic inhibition of calcium carbonate formation by waste water constituents. In: Rubin AJ (ed) Chemistry of waste water technology. Ann Arbor Sci 31–58
Reddy MM, Gaillard WD (1981) Kinetics of calcium carbonate (calcite)-seeded crystallization: Influence of solid/solution ratio on the reaction rate constant. J Colloid Interface Sci 80:171–178
Reddy MM, Nancollas GH (1971) The crystallization of calcium carbonate I. Isotopic exchange and kinetics. J Colloid Interface Sci 36:166–172
Reddy MM, Plummer LN, Busenberg E (1981) Crystal growth of calcite from calcium bicarbonate solutions at constant PCO_2 and 25°C: a test of a calcite dissolution model. Geochim Cosmochim Acta 45:1281–1289
Romanek CS, Gauldie RW (1996) A predictive model of otolith growth in fish based on the chemistry of the endolymph. Comp Biochem Physiol A-Physiol 114:71–79
Romanek CS, Grossman EL, Morse JW (1992) Carbon isotopic fractionation in synthetic aragonite and calcite: effects of temperature and precipitation rate. Geochim Cosmochim Acta 56:419–430
Scholle PA, Halley RB (1985) Burial diagenesis: out of sight, out of mind. In: Schneidermann N, Harris PM (eds) Carbonate cements. Soc Econ Paleon Mineralogists Spec Pub 36:309–334
Tai CY, Chen F-B (1998) Polymorphism of $CaCO_3$ precipitated in a constant-composition environment. Am Inst Chem Eng J 44:1790–1798
Walter LM (1986) Relative efficiency of carbonate dissolution and precipitation during diagenesis: a progress report on the role of solution chemistry: Roles of organic matter in mineral diagenesis. Gautier DL (ed) Soc Econ Paleon Mineralogists Spec Pub 38:1–11
Wiechers HNS, Sturrock P, Marais GVR (1975) Calcium carbonate crystallization kinetics. Water Res 9:835–845
Wiltschko DV, Morse JW (2001) Crystallization pressure versus "crack-seal" as the mechanism for banded veins. Geology 29:79–82
Wray JL, Daniels F (1957) Precipitation of calcite and aragonite. Am Chem Soc J 79:2031–2034
York D (1966) Least squares fitting of a straight line. Can J Phys 44:1079–1086